Development of Automatic Techniques for Segmentation of Brain Tissues from Multispectral MR Images

Zhengrong Liang[1], *Decheng Wang*[+], *Jinhan Ye and Donald Harrington*

Department of Radiology, State University of New York, Stony Brook, NY 11794

Department of Mathematics and Statistics, University of Massachusetts, Amherst, MA 01003[+]

Abstract

Automatic segmentation of brain tissues from multispectral magnetic resonance (MR) images (acquired as relaxation time T_1, T_2, and proton density P_D weighted by selecting appropriate settings of T_E and T_R, the spin-echo delay time and repetition time of a pulse sequence) requires automating the following steps: (1) compensation for image-intensity variation of a same tissue type induced by radiofrequency inhomogeneity across field-of-view; (2) stripping away image pixels which represent skull and scalp; and (3) estimation of model parameters (or training samples) such as image-intensity mean and variance for each tissue type and correlation coefficients for that tissue type among the three spatially-registered images (acquired in a very short time period). This proposed automatic approach first strips away the pixels of skull and scalp. The stripping is performed by detecting radially the pixels of inner-skull margin from the T_2 weighted transaxial image and applying the detected margin to remove the pixels of skull and scalp in the T_1 and P_D weighted transaxial images as well. The approach then determines the intensity-variation map within the margin from each stripped image and compensates for the variation by dividing that image by the determined map. Finally the approach estimates the model parameters by fitting the image data into a multivariate mixture. The fitting is performed by a maximum-likelihood estimator. The above three steps have been successfully implemented by a computer. The automatic approach was tested by a set of three MR images acquired by a 1.5 Tesla whole body scanner from a head. The removal of skull and scalp was very satisfactory. The compensation for the intensity variation improved significantly the estimation of model parameters.

I. INTRODUCTION

Segmentation of brain tissues from neurological magnetic resonance (MR) images is a necessary and non-trivial procedure for (1) volume measurement, (2) three dimensional display, and (3) feature analysis. These three techniques have clinical applications in diagnosis of disorders, such as Alzheimer's disease, epilepsy, atrophy, schizophrenia, and multiple sclerosis [4,8-10]. One of the major advantages in using MR images over computed tomography (CT) data which has been attempted previously [6,17] for brain-tissue segmentation, is the visually differentiable of gray and white matters, in addition to low radiation and multispectral characteristics of relaxation time T_1, T_2, and proton density P_D information [16,19]. An automatic procedure is clinically demanded for consistency of data analysis and reduction of processing time.

Great research effort has recently been devoted to develop automatic approaches for the tissue segmentation, as reported in the review articles [2,7]. We have previously studied a statistical automatic approach for estimation of model parameters (such as pixel mean, variance, and correlation coefficient) for each tissue type [11,12] and segmentation of tissue types on an image array [13-15]. In this work, that study is extended to investigate the automation of (a) correction for radiofrequency (RF) inhomogeneity across field-of-view (FOV) [1,3,5,16,18] and (b) removal of skull and scalp prior to segmenting the brain tissues. That study is further extended to investigate the gain in parameter estimation by the correction of the RF inhomogeneity.

II. METHODS

The proposed automatic approach first strips away pixels of skull and scalp in acquired images and then compensates for intensity variation of a same tissue type induced by the RF inhomogeneity for each image.

A. *Stripping away Pixels of Skull and Scalp*

The stripping away the pixels of skull and scalp in acquired images is performed by: (1) sampling 256 radii, each consisting of 128 pixels, from the center of the T_2 weighted transaxial image (see the middle of Fig.1), and laying them in rows to form a new radial image (see the left of Fig.2), where a bilinear interpolation in two dimensions is used; (2) identifying the pixel of skin/air boundary on each row from right to left (on the radial image) by threshold of pixel value greater than 100 (air background); (3) advancing 30 pixels left in that row from the skin/air boundary and then searching from left to right for the pixel of inner-skull margin which is less than 65% of a running average of the previous ten pixels in that row; (4) smoothing the determined radial inner-skull margin (see the middle of Fig.2); (5) converting the smoothed radial inner-skull margin back to the rectangular coordinates of the original image (see the right of Fig.2); and (6) removing the pixels of skull and scalp outside the inner-skull margin in the acquired T_1, T_2, and P_D weighted images (see Fig.3).

1) This work was supported by Grant #HL44194, awarded by the National Heart, Lung, and Blood Institute.

0-7803-2544-3/95 $4.00 © 1995 IEEE

B. *Correcting for RF Inhomogeneity*

The correcting for the RF inhomogeneity is performed by first computing the map of the intensity variation across the FOV for each stripped image of Fig.3 and then dividing that image by the computed map.

The intensity-variation map is computed by: (1) calculating four radial averages along the positive and negative directions of the central row and column on each image of Fig.3; (2) differencing the two averages in that row and column, respectively; (3) determining the "intensity-invariant" direction by that row (or column) which has a smaller average difference, i.e., the direction with smaller difference of averages has less intensity variation, as compared to the other direction with larger difference of averages; (4) setting a minimum/maximum range for each row (or column) in the intensity-invariant direction by 0.8 and 1.2 times of the average along that row (or column), where the computed average along the direction with less intensity variation is expected to be more reliable than that computed along the other direction; (5) truncating the pixel values in that row (or column) into that range; and (6) smoothing the truncated image by a 9×9 window five to ten times to obtain the map which is expected to vary slowly across the FOV (see Fig.4); in the smoothing, when a part of the window is outside the determined margin, this part will be ignored in calculating the average for the pixel at the window center which is limited inside the margin.

The computed intensity-variation maps of Fig.4 are scaled by dividing their maximal values, respectively, before being used to compensate for the variation.

The gain in estimation of model parameters by correcting for the RF inhomogeneity is studied by first applying the automatic estimation approach [11,12] to both the original images of Fig.3 and the corrected images of Fig.5, respectively, and then comparing the results.

C. *Estimating Model Parameters*

The automatic estimation approach fits the three-image data into a multivariate mixture for the model parameters: (1) the number of components in the mixture determines the number of tissue types; and (2) each component is a multivariate normal function which characterizes a tissue type by its three pixel means, three variances, and three correlation coefficients among the three spatially registered images (which are acquired in a very short time period). The three variances are the diagonal elements of the covariance matrix of the multivariant function. The three correlation coefficients make up the three off-central elements. The covariance matrix is symmetrical and positive definite.

These model parameters in the mixture are estimated by maximum likelihood (ML) combining with an iterative expectation-maximization (EM) algorithm [11,12]. The number of tissue types is determined by an information criterion which is based on a Bayesian inference [11,12].

The above three steps of removal of skull and scalp, correction of RF inhomogeneity and estimation of model parameters are implemented automatically by a computer. Thereafter, segmentation of the brain tissues is straightforward [13]. As an example, a ML segmentation is employed to investigate the gain by the correction of RF inhomogeneity.

III. RESULTS

A set of three images was acquired by a 1.5 Tesla GE whole body scanner from a head and used to test the above described automatic approach. Figure 1 shows a selected slice each from the acquired images, respectively. The slice is 5 mm thick. The space between slices is 1 mm. The FOV is 20 cm over a 256×256 image array. The raw data were sampled by 192 phase lines with 256 points on each line. A spin-echo pulse sequence was used. On the left is the T_1 weighted image with T_E/T_R = 18/800 in units of msec (T_E: spin-echo delay time, T_R: repetition time of a pulse sequence). In the middle is the T_2 weighted image with T_E/T_R = 95/4000. And on the right is the P_D weighted image with T_E/T_R = 19/2500.

The detection of the inner-skull margin is described by Fig.2. On the left is the radial image sampled from the T_2 weighted image. In the second left is the first-order differentiation of the radial image along the horizontal direction. It is easy to see that the cerebrospinal fluid (CSF) space causes difficulty for detection of the margin when search starts from the beginning to the right. Attempt has been made to avoid the difficulty by starting the search after the CSF space on the radial image [16]. The attempt does not completely overcome the difficulty because the CSF space and the inner-skull margin vary significantly from case to case on the sampled radial images. We proposed an alternative technique to avoid the difficulty as described above. The technique first searches for the skin/air boundary starting from right to left. Since the skin and air have a huge contrast, their boundary can be easily detected. Then the technique considers the fact that the inner-skull margin has a relatively fixed distance from the skin/air boundary on the radial image. So the proposed technique identifies the margin from left to right at those starting points (on the rows of the radial image) which have a fixed distance from their detected skin/air boundary and therefore avoid the difficulty completely. In the middle of Fig.2 are the detected inner-skull margin and skin/air boundary.

Up to this point, the advantage of using the radial image for detection of the inner-skull margin is clearly seen. The detected margin is one dimensional and can be smoothed easily, as shown in the second right of Fig.2. On the right of that figure are the inner-skull margin and skin/air boundary converted back from the radial representation to the original rectangular coordinates.

Figure 3 shows the acquired images of Fig.1 after the skull and scalp have been removed. The performance of the

automatic removal of the skull and scalp is very satisfactory.

Figure 4 represents the computed intensity-variation maps from the stripped images of Fig.3, respectively. It is interesting to see that the maps of T_1, T_2, and P_D weighted images are significantly different, in contrast to our expectation. We expect that the maps would be similar because their images were acquired by the same scanner in a very short time period. This experiment indicates that the correction for the RF inhomogeneity should be performed for each image, respectively, and the intensity-variation map should be determined from that image to be corrected by the map.

The intensity-variation maps of Fig.4 were scaled by dividing the maps by their maximal values, respectively, before being used to correct for the RF inhomogeneity. The corrected images are shown in Fig.5. These images were obtained by dividing the original images of Fig.3 by their scaled maps of Fig.4, respectively. The uniformity of image intensities of a same tissue type is significantly improved across the FOV. This is especially noticeable in the corrected T_1 and P_D weighted images. Figure 6 makes a clear contrast between the corrected images and the original images by showing their intensity profiles of one-pixel width drawn vertically along a line just outside the left ventricle. The dotted lines represent the profiles of the original images, respectively. The solid lines are the profiles of the corrected images. And the broken lines are the profiles of the intensity-variation maps.

Figures 7 and 8 contrast the ML segmentation between the original images of Fig.3 and the corrected images of Fig.5. The gain by the correction of RF inhomogeneity is clearly seen. In the segmentation from the original images, the gray and white matter are not distinguishable and are a mixture of two parts solely due to the RF inhomogeneity. The CSF space was successfully segmented because its strong signal in the T_2 weighted image is not distorted much by the small RF inhomogeneity in that image and its weak signal in the T_1 and P_D weighted images has small variation even if the RF inhomogeneity there is severe. The CSF, gray and white matter all were successfully segmented after the correction of RF inhomogeneity.

IV. CONCLUSIONS

An automatic approach has been described which aims to facilitate the segmentation of brain tissues from multispectral MR images. The images can be either acquired as T_1, T_2, and P_D weighted by selecting appropriate T_E and T_R settings, or computed as T_1, T_2, and P_D intrinsic parameters from acquired images [14]. The approach first strips away the skull and scalp by detecting the inner-skull margin using the T_2 weighted transaxial image. The approach then compensates for the intensity variation of a same tissue type across the FOV induced by the RF inhomogeneity. Finally the approach estimates the model parameters for the brain tissues using the corrected image data. These three automatic steps provide a basis for the automatic segmentation of the tissues on the image array (or patient space), as described in our previous work [15], as well as others [2,7]. The removal of skull and scalp is very satisfactory. The correction of RF inhomogeneity improves significantly the tissue segmentation. The correction is very necessary for quantitative volume analysis as demanded in clinical applications [4,8-10]. It is highly recommended to compute the intensity-variation map for each individual image, respectively, for the correction of RF inhomogeneity.

V. ACKNOWLEDGMENT

The authors appreciate Dr. Clemente Roque and Dr. HaiFang Li for their assistance in preparing this manuscript.

VI. REFERENCES

[1] L. Axel, J. Costantini and J. Listerud, "Intensity Correction in Surface-Coil MR Imaging", Am J Roentgenology, **128**: 418-420, 1987

[2] J.C. Bezdek, L.O. Hall and L.P. Clarke, "Review of MR Image Segmentation Techniques Using Pattern Recognition", Med Physics, **20**: 1033-1048, 1993

[3] W.W. Brey and P.A. Narayana, "Correction for Intensity Falloff in Surface Coil MR Imaging", Med Physics, **15**: 241-245, 1988

[4] G.D. Cascino, C.R. Jack, J.E. Parisi, et al., "MR Imaging-Based Volume Studies in Temporal Lobe Epilepsy: Pathological Correlations", Ann Neurology, **30**: 31-36, 1991

[5] B.M. Dawant, A.P. Zijdenbos and R.A. Margolin, "Correction of Intensity Variations in MR Images for Computed-Aided Tissue Classification", IEEE TMI, **12**: 770-781, 1993

[6] J.M. DeLeo, M. Schwartz, H. Creasey, et al., "Computer-Assisted Categorization of Brain CT Pixels into CSF, White Matter, and Gray Matter", Comput Biomed Res, **18**: 79-88, 1985

[7] L.O. Hall, A.M. Bensaid, L.P. Clarke, et al., "A Comparison of Neural Network and Fuzzy Clustering Techniques in Segmenting MR Images of the Brain", IEEE TNN, **3**: 672-683, 1992

[8] C.R. Jack, F.W. Sharbrough, C.K. Twomey, et al., "Temporal Lobe Seizures: Lateralization with MR Volume Measurements of the Hippocampal Formation", Radiology, **175**: 423-429, 1990

[9] M.I. Kohn, N.K. Tanna, G.T. Herman, et al., "Analysis of Brain and CSF Volumes with MR Imaging, Part I. Methods, Reliability, and Validation", and "Part II. Aging and Alzheimer Dementia", Radiology, **178**: 115-130, 1991

[10] T. Lencz, G. McCarthy, R.A. Bronen, et al., "Quantitative Magnetic Resonance Imaging in Temporal Lobe Epilepsy: Relationship to Neuropathology and Neuropsychological Function", Ann Neurology, **31**: 629-637, 1992

[11] Z. Liang, R.J. Jaszczak and R.E. Coleman, "On Reconstruction and Segmentation of Piecewise Continuous Images", in Proc IPMI, **12**: 94-104, 1991

[12] Z. Liang, R.J. Jaszczak and R.E. Coleman, "Parameter Estimation of Finite Mixture Using the EM Algorithm and Information Criteria with Application to Medical Image Processing", IEEE TNS, **39**: 1126-1133, 1992

[13] Z. Liang, "Tissue Classification and Segmentation of MR Images", IEEE EMB Magazine, 12: 81-85, 1993

[14] Z. Liang and J.R. MacFall, "Automatic Tissue Segmentation from Computed Intrinsic MR Images", in Proc SMRM, 2: 695, 1993

[15] Z. Liang, J.R. MacFall and D.P. Harrington, "Parameter Estimation and Tissue Segmentation from Multispectral MR Images", IEEE TMI, 13: 441-449, 1994

[16] K.O. Lim and A. Pfefferbaum, "Segmentation of MR Brain Images into CSF Spaces, White and Gray Matter", JCAT, 13: 131-145, 1989

[17] A. Pfefferbaum, L.M. Zatz and T.L. Jernigan, "Computer-Interactive Method for Quantifying CSF and Tissue in Brain CT Scans: Effects of Aging", JCAT, 10: 571-578, 1980

[18] A. Simmons, S.R. Arridge, G.J. Barker, et al., "A Multi-Stage Pipeline for Segmentation of Neurological MRI Data", Proc SMRM, 3: 696, 1993

[19] M.W. Vannier, R.L. Butterfield, D. Jordan, et al., "Multispectral Analysis of MR Images", Radiology, 154: 221-224, 1985

Fig.1: A set of T_1 (left, T_E/T_R = 18/800), T_2 (middle, T_E/T_R = 95/4000), and P_D (right, T_E/T_R = 19/2500) weighted transaxial brain images.

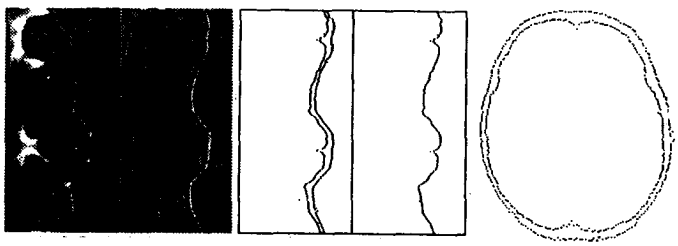

Fig.2: The radial image sampled from the T_2 weighted image (left), its first-order differentiation along horizontal axis (second left), the detected inner-skull margin and skin/air boundary from the radial image (middle), the smoothed inner-skull margin (second right), and the inner-skull margin and skin/air boundary represented in the rectangular coordinates (right).

Fig.3: The acquired images of Fig.1 after stripping away the skull and scalp.

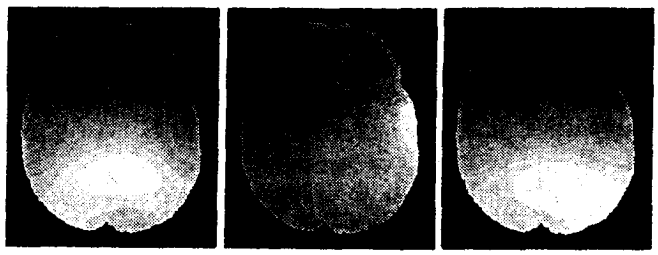

Fig.4: The computed intensity-variation maps of a same tissue type across the FOV induced by the RF inhomogeneity from the stripped images of Fig.3.

Fig.5: The acquired images of Fig.3 after correction of the RF inhomogeneity.

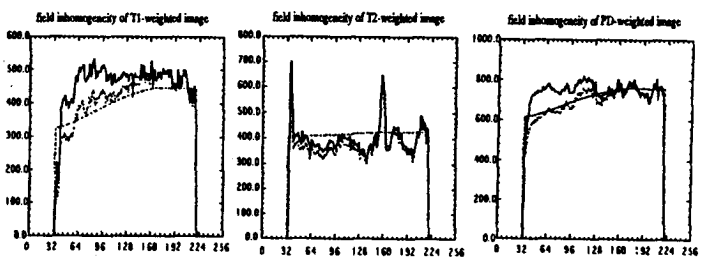

Fig.6: The intensity profiles drawn vertically along a line near the left ventricle from the original images of Fig.3 (dotted lines), the corrected images of Fig.5 (solid lines), and the maps of Fig.4 (broken lines).

Fig.7: The segmented mixture of gray and white matter (left and middle) and CSF space (right) from the original images of Fig.3.

Fig.8: The segmented gray (left) and white (middle) matter and CSF space (right) from the corrected images of Fig.5.